



Cite this: *Phys. Chem. Chem. Phys.*,  
2014, 16, 22364

## Vibrational spectra and structures of neutral Si<sub>6</sub>X clusters (X = Be, B, C, N, O)†

Nguyen Xuan Truong,<sup>a</sup> Marco Savoca,<sup>a</sup> Dan J. Harding,<sup>bc</sup> André Fielicke<sup>a</sup> and Otto Dopfer<sup>\*a</sup>

Neutral silicon clusters doped with first row elements (Si<sub>6</sub>X) have been generated (X = B, C, N, O) and characterized by infrared–ultraviolet (IR–UV) two-photon resonance-enhanced ionization spectroscopy (X = C, O) and quantum chemical calculations (X = Be, B, C, N, O, Si). In the near threshold UV photoionization, the ion signal of specific cluster sizes can be significantly enhanced by resonant excitation with tunable IR light prior to UV irradiation, allowing for the measurement of the IR spectra of Si<sub>7</sub>, Si<sub>6</sub>C, and Si<sub>6</sub>O clusters. Structural assignments are achieved with the help of a global optimization procedure using density functional theory (DFT). The most stable calculated structures show the best agreement between predicted and measured spectra. The dopant atoms in the Si<sub>6</sub>X clusters have a negative net charge and the Si atoms act as electron donors within the clusters. Moreover, the overall structures of the Si<sub>6</sub>X clusters depend strongly on the nature of the dopant atom, *i.e.*, its size and valency. While in some of the Si<sub>6</sub>X clusters one Si atom in Si<sub>7</sub> is simply substituted by the dopant atom (X = Be, B, C), other cases exhibit a completely different geometry (X = N, O). As a general trend, doping of the Si<sub>7</sub> cluster with first-row dopants is predicted to shift the optically allowed electronic transitions into the visible or even near-IR spectral range due to symmetry reduction or the radical character of the doped cluster.

Received 31st July 2014,  
Accepted 27th August 2014

DOI: 10.1039/c4cp03414g

www.rsc.org/pccp

### 1. Introduction

Small silicon clusters have attracted great interest in the current move towards nanoelectronics.<sup>1</sup> At the nanometer scale, where every atom counts, structure determination plays a crucial role. It has been shown that by changing the cluster size or dopant species, new stable nanostructures with tailored chemical, optical, or magnetic properties can be obtained.<sup>2–8</sup> While pure silicon clusters have been often studied as a test model system for quantum theories, doped silicon clusters have even more potential for applications in numerous fields of materials science.<sup>9</sup> Charged Si-containing clusters have been widely investigated, in part because they can be easily manipulated and detected using mass spectrometric methods. Gas-phase neutral clusters are more difficult to detect and thus less is known about them. Infrared photodissociation has been used for neutral clusters, in combination with ionization, to allow for mass spectrometric analysis of the cluster sizes.<sup>10–12</sup> Besides this, there have been

two major spectroscopic methods used that directly influence the ionization process of the neutral clusters by absorption of IR photons, namely, infrared resonance-enhanced multiple photon ionization (IR–REMPI)<sup>13</sup> and infrared–ultraviolet two-color ionization (IR–UV2CI).<sup>14</sup> Generally, they are applied to cluster distributions and take advantage of the change in charge state resulting from photoionization of the cluster. In IR–REMPI, several hundred IR photons usually need to be absorbed in order to induce ionization. The method therefore works only for a limited range of very strongly bound systems like fullerenes and clusters of certain (refractory) metals and metal compounds.<sup>13,15</sup> The multiple photonic character can also make the interpretation of IR–REMPI spectra more difficult. Consequently, elaborate models have been applied to gain more insight into the multiple photon excitation mechanism.<sup>16,17</sup> IR–UV2CI, on the other hand, is more widely applicable. In IR–UV2CI experiments, a cluster first resonantly absorbs one or more IR photons to make a vibrational transition. It is then post-ionized by absorbing a single UV photon and finally detected in a mass spectrometer. The energy of the UV photon is chosen to be close to the ionization threshold, such that without the IR photons almost no ion signal is observed. Because only a few IR photons are involved in an IR–UV2CI measurement, the resulting vibrational spectra are closely related to the linear absorption spectra and hence much better resolved than typical IR–REMPI spectra. However, as the ionization energy (IE) of clusters is

<sup>a</sup> Institut für Optik und Atomare Physik, Technische Universität Berlin, Hardenbergstraße 36, D-10623 Berlin, Germany. E-mail: dopfer@physik.tu-berlin.de

<sup>b</sup> Institut für Physikalische Chemie, Georg-August-Universität Göttingen, Tammannstraße 6, D-37077 Göttingen, Germany

<sup>c</sup> Department of Dynamics at Surfaces, Max-Planck-Institut für Biophysikalische Chemie, Am Fassberg 11, D-37077 Göttingen, Germany

† Electronic supplementary information (ESI) available. See DOI: 10.1039/c4cp03414g

usually size-dependent, only selected cluster sizes may be probed with a given UV photon energy.

Whereas an enormous amount of theoretical work on small doped silicon clusters is available (*e.g.*, ref. 12, 18–34), only a few experiments have been reported in the gas phase.<sup>8,14,35–38</sup> By sequential doping of silicon clusters with carbon atoms, *i.e.*, for  $\text{Si}_m\text{C}_n$  with  $m + n = 6$ , we recently observed a systematic transition from one-dimensional geometries for pure  $\text{C}_6$  to three-dimensional structures for pure  $\text{Si}_6$ .<sup>38</sup> In this study, we present complementary experimental and theoretical results on silicon clusters doped with first row elements ( $\text{Si}_6\text{X}$ , with  $\text{X} = \text{Be}, \text{B}, \text{C}, \text{N}, \text{O}$ ). Structures of these clusters have been predicted using DFT-based basin hopping (BH) global optimization.<sup>39,40</sup> Refined DFT calculations have been performed for the most stable isomers, yielding detailed information such as vibrational spectra, excitation and ionization energies, HOMO–LUMO gaps, and natural charge populations. By comparing the IR–UV2CI spectra of  $\text{Si}_6\text{C}$  and  $\text{Si}_6\text{O}$  clusters to the calculations, the corresponding structures are assigned.

## II. Experimental and computational methods

The experimental setup used for IR–UV2CI spectroscopy has been described in detail elsewhere.<sup>14,38,41</sup> Briefly, Si-rich  $\text{Si}_m\text{X}_n$  clusters are produced by laser ablation of a pure silicon rod within a pulsed flow of He gas (containing 1%  $\text{CH}_4$ , 0.7%  $\text{N}_2$ , or 0.07%  $\text{O}_2$ , depending on the desired dopant) and thermalized to  $\sim 100$  K in a liquid-nitrogen cooled expansion channel. For the case of boron, a dual target source with pure He carrier gas is used.<sup>42</sup> After passing through a skimmer, the neutral  $\text{Si}_m\text{X}_n$  clusters are overlapped with counter-propagating IR radiation from the ‘Free Electron Laser for Infrared eXperiments’ FELIX and then post-ionized by an unfocused  $\text{F}_2$  laser (7.87 eV) in the extraction zone of a reflectron time-of-flight mass spectrometer.

Fig. 1 shows typical mass spectra of the doped silicon clusters exposed to either UV only or the IR and UV lasers. The ion signal intensities depend strongly on the cluster size and the corresponding ionization energies. For clusters of specific sizes, with an IE close to the photon energy of the ionizing laser, prior resonant excitation with IR photons from a pulse of FELIX may enhance the ionization efficiency (Fig. 1d). Therefore, the enhancement of the ion yield as a function of the IR wavelength largely reflects the vibrational absorption spectrum of the original neutral cluster. Further details of the IR–UV ionization mechanism are provided in ref. 14 and 41.

The reported IR spectra are obtained from the relative ionization enhancement determined by the difference of the ion  $\text{IR}^{\text{on}}$  and  $\text{IR}^{\text{off}}$  signals normalized with the  $\text{IR}^{\text{off}}$  signal and the IR photon flux. The observed widths of the bands of  $15\text{--}45\text{ cm}^{-1}$  arise from a combination of unresolved rotational structure, sequence hot band transitions involving low-frequency modes, the FELIX bandwidth (*ca.* 0.5–1% full width at half maximum (FWHM) of the central wavelength), and possibly the multiple photon absorption process.

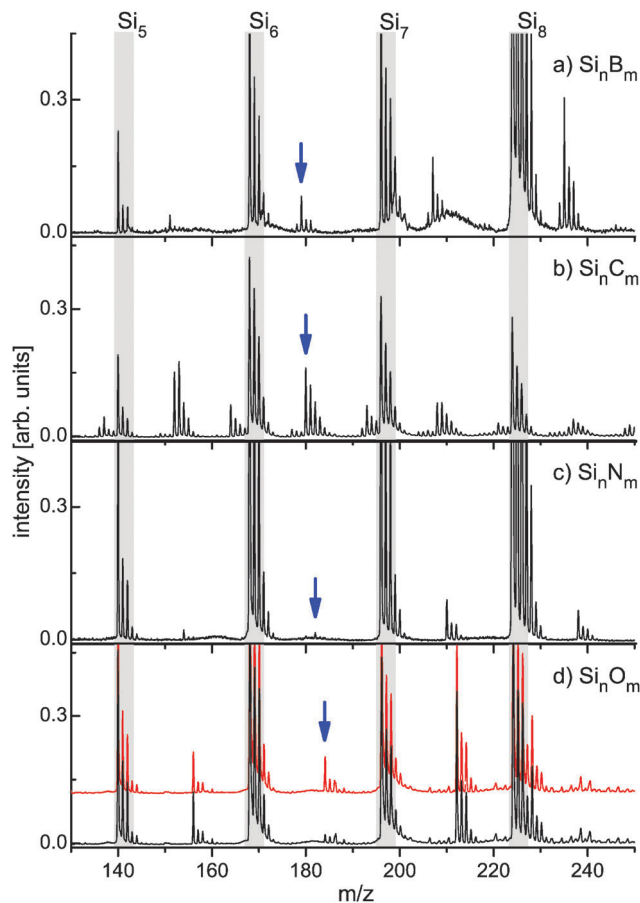


Fig. 1 Mass spectra (black lines) of doped silicon clusters  $\text{Si}_n\text{X}_m$  ( $n = 5\text{--}8$ ,  $m = 1\text{--}2$ , and  $\text{X} = \text{B}, \text{C}, \text{N}, \text{O}$ ) obtained by ionization with an  $\text{F}_2$  laser. The  $\text{Si}_6\text{X}$  clusters are marked by arrows. For the case of oxygen (d), an additional mass spectrum (red line) is included to highlight the enhancement of the  $\text{Si}_6\text{O}$  ion yield with the presence of IR radiation at  $865\text{ cm}^{-1}$ . For each group of signals, the leading mass peak corresponds to the all- $^{28}\text{Si}$  isotopologue, while most of the adjacent peaks are assigned to other Si isotopologues.

Quantum chemical calculations have been performed to aid in the assignment of the cluster structures, to give more insight into their physical and chemical properties, and to serve as a guide for future experiments. By comparing the measured IR spectrum with the calculated spectra of the low lying isomers, the geometric structure of the observed cluster can be determined. Furthermore, an estimate of the IE of the clusters of interest is crucial for choosing the appropriate UV photon energy in the IR–UV2CI experiments.

For each cluster size, many geometric configurations are possible. In an effort to thoroughly explore these possibilities, we have employed the basin hopping technique,<sup>40,43–46</sup> which has proven to be an effective stochastic global search algorithm. Details of our implementation have been described elsewhere.<sup>39</sup> Basically, there are two main steps. First, for each cluster thousands of structures are evaluated in terms of the total energy by a BH algorithm coupled with DFT calculations at the RI-BP86/def-SVP level using Turbomole V6.3.1.<sup>47–49</sup> The BH uses a Monte Carlo (MC) simulation at a constant temperature

of 1200 K and consists of 1500 MC steps. New structures are generated with the significant structure variant using single-atom moves, followed by all-atom displacements at every five steps.<sup>39</sup> The self-consistent field (SCF) convergence criterium of  $10^{-5}$  hartree on the total energy was chosen. The relatively low computational cost enables the BH approach to explore a large number of test structures. Second, the structures of interest, *e.g.*, the first 10–15 different low-energy isomers, are refined with different functionals, *i.e.*, the B3LYP/cc-pVTZ, TPSS/def2TZVP, and BP86/SVP levels, with SCF convergence conditions of better than  $10^{-8}$  hartree and the resolution-of-the-identity approximation as implemented in the Gaussian 09 package.<sup>50</sup> We note that these methods have proven reliable for silicon-containing clusters reported previously.<sup>14,38</sup> At such levels, detailed information about the linear IR absorption spectra, ionization energies, and natural bond orbital populations is obtained. If not stated otherwise, all relative energies include zero-point vibrational energy corrections except for the vertical ionization energy (VIE) values. The electronic ground state of the considered clusters has the lowest possible spin multiplicity. The electronic transitions of the ground state structures are calculated at the CAM-B3LYP/cc-pVTZ level<sup>50</sup> to explore their electronic structure. To facilitate convenient comparison with the experimental spectra, the theoretical IR stick absorption spectra are convoluted with a Gaussian line profile using a FWHM of  $15\text{ cm}^{-1}$ . The reported vibrational frequencies are unscaled.

### III. Results and discussion

#### A. Predicted structures

The five lowest-energy isomers of the  $\text{Si}_6\text{X}$  clusters identified using the global optimization procedure described in Section II are shown in Fig. 2. The energetic, vibrational, and electronic parameters of the most stable isomers are listed in Tables 1–3, respectively. We note that the three functionals predict the same ground state structures while for higher-energy isomers the energetic ordering is only slightly changed. Therefore, the optimized geometric and vibrational parameters obtained with the B3LYP/cc-pVTZ level will be used in the following discussion.

Interestingly, for the most stable configurations of  $\text{Si}_6\text{Be}$  ( $^1\text{A}_1$ ),  $\text{Si}_6\text{B}$  ( $^2\text{A}'$ ), and  $\text{Si}_6\text{C}$  ( $^1\text{A}_1$ ), the dopant atom simply replaces one Si atom of pure  $\text{Si}_7$  ( $D_{5h}$ ), leading to a reduction of the molecular symmetry. On the contrary, completely new structures are formed for  $\text{Si}_6\text{N}$  ( $^2\text{A}_2$ ) and  $\text{Si}_6\text{O}$  ( $^1\text{A}$ ). In most cases, the dopant atom prefers a location surrounded by as many Si atoms as possible. The  $\text{Si}_6\text{O}$  isomers are, however, most stable with an O atom on the edge of a low-energy isomer of the  $\text{Si}_6$  cluster. Our numerical results are in good agreement with earlier calculations of  $\text{Si}_6\text{O}$ <sup>24</sup> and  $\text{Si}_6\text{B}$ .<sup>51</sup> Furthermore, to the best of our knowledge, we have found a new lowest-energy structure for the  $\text{Si}_6\text{N}$  cluster (**d0**, Fig. 2), which is significantly lower in energy (0.49 eV at the B3LYP/cc-pVTZ level) than the best structure reported previously (**d2**, Fig. 2 and, *e.g.*, ref. 52).

While the **d2** structure is formed by the substitution of a Si atom, our new **d0** structure has a completely different geometry with only one Si atom attached to the divalent N atom, leading to an isocyanide-type linear configuration. Calculations with different methods, *e.g.*, genetic algorithms,<sup>53</sup> functionals, and basis sets (not shown here) support our finding.

If one only considers the substitutional isomers of  $\text{Si}_7$ , there are two possible places to exchange a Si atom for a dopant atom, namely, in the ring and at the apexes of the bipyramid. When located in the ring,  $\text{Si}_6\text{Be}$ ,  $\text{Si}_6\text{B}$ , and  $\text{Si}_6\text{N}$  form  $C_{2v}$  symmetry isomers (**a0**, **b4**, and **d2**, Fig. 2), while  $\text{Si}_6\text{C}$  has  $C_s$  symmetry (**c3**, Fig. 2). When the dopant atom is placed at an apex of the bipyramid,  $\text{Si}_6\text{C}$  (**c0**, Fig. 2) and  $\text{Si}_6\text{N}$  ( $E_{\text{rel}} = 1.69\text{ eV}$ , not shown) form highly symmetrical configurations ( $C_{5v}$ ), whereas the other clusters form lower symmetry  $C_s$  structures. The shortest Si–X bond lengths (in Å) in the most stable  $\text{Si}_6\text{X}$  structures are 2.16 (Be), 2.08 (B), 2.05 (C), 1.58 (N), and 1.66 (O).

#### B. Ionization energetics

The value of the ionization energy of a cluster compared to the UV photon energy used to finally ionize the cluster determines the success of an IR–UV2CI measurement. Experiments on neutral Si clusters suggest that the IE has to be within 0.1–0.2 eV of the UV photon energy to obtain sufficient enhancement in the ionization efficiency by resonant absorption of IR photons.<sup>14,41</sup> This also explains that in case of the  $\text{Si}_m\text{C}_n$  ( $m + n = 6$ ) clusters no effect on the ionization efficiency of  $\text{Si}_3\text{C}_3$  could be observed due to its high IE (9.12 eV) compared to the photon energy of 7.87 eV used for ionization.<sup>38</sup> The calculated adiabatic and vertical ionization energies and binding energies of the most stable  $\text{Si}_6\text{X}$  clusters with different functionals and basis sets are shown in Table 1. Note that our calculated values for  $\text{Si}_7$  are in excellent agreement with experiments.<sup>54,55</sup>

Except for the case of  $\text{Si}_6\text{N}$  with a calculated VIE of  $\sim 7.5\text{ eV}$ , the IEs of other clusters are close to the  $\text{F}_2$  laser photon energy of 7.87 eV, making them promising candidates for IR–UV2CI spectroscopy using such a UV laser. Indeed, experimental IR–UV2CI spectra have been successfully recorded for  $\text{Si}_6\text{C}$  and  $\text{Si}_6\text{O}$  and are shown in Fig. 3.  $\text{Si}_6\text{N}$  may need a different experimental approach, as its predicted IE is too high for using an ArF laser (6.4 eV) and no other simple laser source exists in this UV range.

Finally, the binding energy (BE) of the dopant atom to the  $\text{Si}_6$  cluster varies drastically between 2.2 and 8.7 eV depending on the nature of the dopant. While the BEs for the electropositive Be and B dopant atoms are similar or lower than that of Si, those of the more electronegative C, N, and O atoms are strikingly high ( $\sim 8\text{ eV}$ ).

#### C. Electronic properties

Mulliken populations are not very suitable for an analysis of the charge transfer in silicon clusters.<sup>56</sup> We have therefore used natural bond orbital concepts<sup>57</sup> to analyze the most stable  $\text{Si}_6\text{X}$  structures. The natural electronic configurations and natural populations are detailed in Table S1 in ESI.† For all of the dopants, the net atomic population is negative ( $-0.166\text{ e}$  (Be),

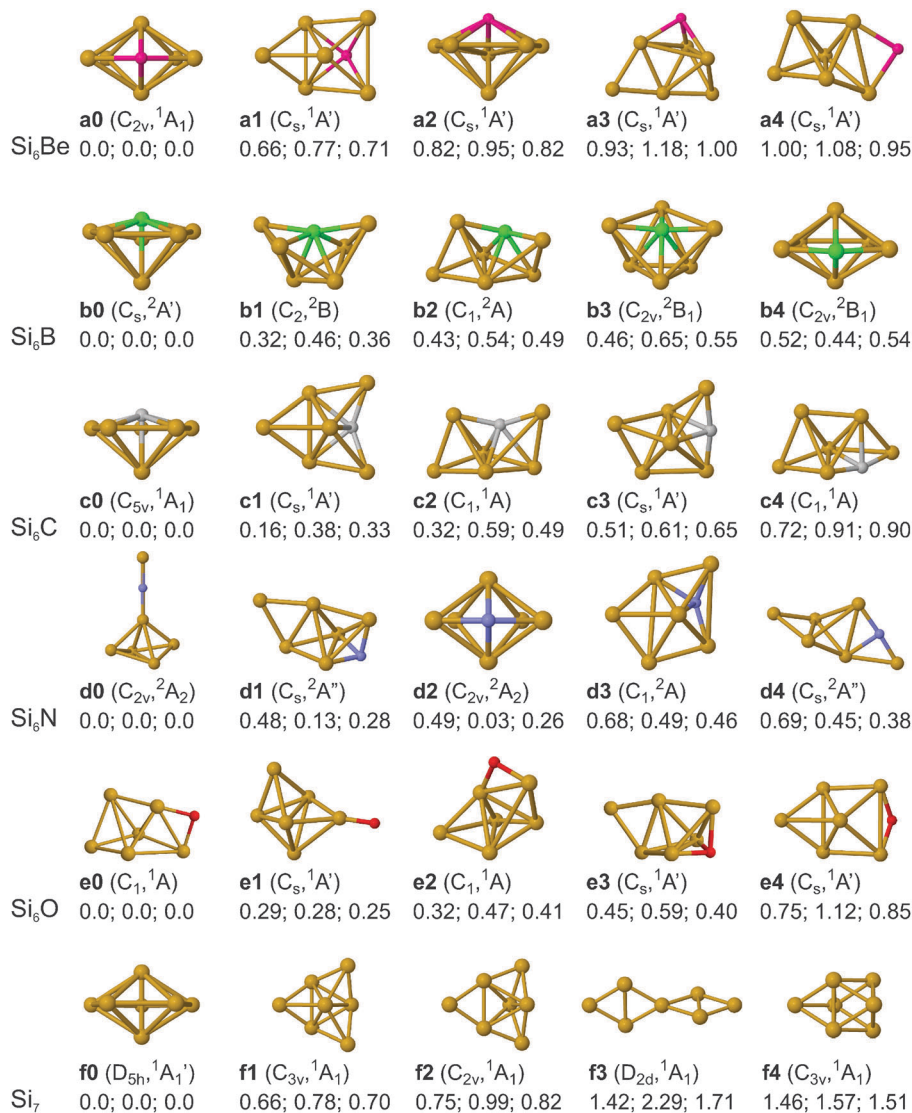


**Fig. 2** Optimized geometries of the first five low-energy  $\text{Si}_6\text{X}$  isomers (with  $\text{X} = \text{Be}, \text{B}, \text{C}, \text{N}, \text{O}, \text{Si}$ ) found with the global optimization algorithm. Point group symmetries and electronic states are given in parentheses. The relative energies  $E_{\text{rel}}$  (in eV) obtained at the B3LYP/cc-pVTZ, TPSS/def2TZVP, and BP86/SVP levels (separated by semicolons, left to right, respectively) are also provided for comparison. Atomic coordinates are available in the ESI.†

**Table 1** Vertical ionization energy (VIE), adiabatic ionization energy (AIE), and binding energy (BE) of the lowest-energy  $\text{Si}_6\text{X}$  isomers (**a0–f0**) calculated at the B3LYP/cc-pVTZ, TPSS/def2TZVP, and BP86/SVP levels (separated by semicolons, left to right, respectively)

Cluster	VIE [eV]	AIE [eV]	BE <sup>a</sup> [eV]
$\text{Si}_6\text{Be}$	7.96; 7.54; 7.80	7.41; 7.37; 7.61	2.25; 2.59; 2.50
$\text{Si}_6\text{B}$	7.96; 8.22; 8.36	7.59; 7.75; 7.84	4.41; 4.76; 4.98
$\text{Si}_6\text{C}$	7.85; 7.82; 8.07	7.55; 7.66; 7.85	7.53; 7.94; 8.26
$\text{Si}_6\text{N}$	7.46; 7.57; 7.72	6.75; 6.93; 7.02	7.40; 5.31; 7.66
$\text{Si}_6\text{O}$	7.99; 8.02; 8.19	7.71; 7.74; 7.93	8.33; 8.69; 8.69
$\text{Si}_7$	7.98; 7.97; 8.23 <sup>b</sup>	7.68; 7.71; 7.93 <sup>b</sup>	4.84; 5.58; 5.40

<sup>a</sup> The binding energy of the  $\text{Si}_6\text{X}$  cluster is given as  $\text{BE} = E(\text{Si}_6) + E(\text{X}) - E(\text{Si}_6\text{X})$ . <sup>b</sup> Experimental value is  $\sim 7.9$  eV.<sup>54,55</sup>

$-1.449$  e (B),  $-1.884$  e (C),  $-1.673$  e (N), and  $-1.241$  e (O)), hinting at the role as electron donors of Si atoms and the ionic characteristics of the Si–X bonding. This has also been

observed for a number of silicon-containing clusters in earlier reports<sup>56,58–60</sup> and is attributed to the low electronegativity of Si. In terms of the natural electronic configurations, most of the dopants considered show an idealized promoted configuration for  $\text{sp}^3$  hybridization, which is most preferable for Si atoms, except for the Be atom which has the valence configuration  $2\text{s}^{0.66}2\text{p}^{1.45}$ .

Excited states of the most stable  $\text{Si}_6\text{X}$  structures are calculated with the TD-DFT method (CAM-B3LYP/cc-pVTZ) as listed in Table 3 for the first three vertical electronic transitions along with the HOMO–LUMO gaps. The corresponding HOMO and LUMO orbitals are shown in Fig. 4. While the HOMO–LUMO gaps are comparable for all  $\text{Si}_6\text{X}$ , their first electronic transitions show a clear trend oscillating between closed- and open-shell clusters, *i.e.*, low excitation energies (0.5–1.2 eV) for open-shell vs. high values ( $> 2.0$  eV) for closed-shell systems. Interestingly,

**Table 2** Vibrational frequencies (in  $\text{cm}^{-1}$ ) of the most stable  $\text{Si}_6\text{X}$  isomers shown in Fig. 2 calculated at the B3LYP/cc-pVTZ level

$\text{Si}_6\text{Be}$ ( $C_{2v}$ )	$\text{Si}_6\text{B}$ ( $C_s$ )	$\text{Si}_6\text{C}$ ( $C_{5v}$ )	$\text{Si}_6\text{N}$ ( $C_{2v}$ )	$\text{Si}_6\text{O}$ ( $C_1$ )	$\text{Si}_7$ ( $D_{5h}$ )
129 (0.6, $a_1$ )	32 (0.6, $a''$ )	105 (0, $e_2$ )	71 (0.6, $b_1$ )	75 (0.3, a)	159 (0, $e_2''$ )
139 (0, $a_2$ )	109 (0.1, $a'$ )	231 (4, $e_1$ )	74 (1.0, $b_2$ )	120 (1, a)	216 (0.04, $e_1'$ )
191 (0.3, $b_1$ )	186 (1.0, $a''$ )	261 (2, $a_1$ )	157 (0.1, $a_1$ )	192 (0.4, a)	217 (1, $a_2''$ )
230 (6, $b_2$ )	212 (9, $a''$ )	274 (0, $e_2$ )	204 (11, $b_1$ )	234 (0.5, a)	271 (0, $e_2''$ )
286 (0.2, $b_2$ )	220 (3, $a''$ )	355 (0.6, $e_1$ )	234 (6, $b_2$ )	240 (0.7, a)	320 (0, $e_1''$ )
289 (2, $b_1$ )	256 (0.1, $a''$ )	421 (0, $e_2$ )	236 (3, $b_1$ )	272 (0.2, a)	333 (0, $e_2''$ )
310 (2, $a_1$ )	282 (0.5, $a'$ )	432 <sup>A</sup> (10, $a_1$ )	264 (0, $a_1$ )	285 (3, a)	350 (0, $a_1'$ )
331 (3, $a_1$ )	286 (2, $a'$ )	552 <sup>B</sup> (50, $e_1$ )	291 (5, $b_2$ )	316 (8, a)	404 (31, $e_1'$ )
336 (0, $a_2$ )	347 (0.1, $a''$ )	553 <sup>B</sup> (69, $a_1$ )	304 (0.01, $a_1$ )	363 (3, a)	421 (0, $a_1'$ )
356 (1, $a_1$ )	386 (0.1, $a'$ )		319 (0, $a_2$ )	376 (11, a)	
408 (3, $b_1$ )	416 (13, $a'$ )		403 (1, $b_1$ )	403 (2, a)	
419 (13, $b_2$ )	451 (0.2, $a''$ )		415 (4, $a_1$ )	422 <sup>D</sup> (8, a)	
424 (15, $a_1$ )	519 (33, $a'$ )		471 (0.2, $b_2$ )	466 <sup>E</sup> (27, a)	
598 (8, $a_1$ )	646 (29, $a'$ )		665 (26, $a_1$ )	572 <sup>F</sup> (15, a)	
617 (0.04, $b_2$ )	652 (28, $a''$ )		1350 (330, $a_1$ )	855 <sup>G</sup> (80, a)	

IR intensities (in  $\text{km mol}^{-1}$ ) and the symmetries of the modes are listed in parentheses. A–G: assigned bands determined by our experiments as shown in Fig. 3.

**Table 3** The first three electronic transitions and HOMO–LUMO gaps for the ground state structures of  $\text{Si}_6\text{X}$  calculated with the CAM-B3LYP/cc-pVTZ method. The respective oscillator strengths  $f$  ( $\times 10^{-3}$ ) are given in parentheses. For the open-shell  $\text{Si}_6\text{B}$  and  $\text{Si}_6\text{N}$ , the HOMO–LUMO gaps for  $\alpha/\beta$  spin components are indicated by up/down arrows

Cluster	Transition energy [eV]	HOMO–LUMO gap [eV]
$\text{Si}_6\text{Be}$ ( <b>a0</b> , $C_{2v}$ , $^1A_1$ )	2.27 (0.0)	5.24
	2.40 (5.7)	
	2.60 (0.4)	
$\text{Si}_6\text{B}$ ( <b>b0</b> , $C_s$ , $^2A'$ )	0.52 (0.1)	6.45 $\uparrow$ 3.83 $\downarrow$
	1.10 (0.1)	
	1.25 (1.5)	
$\text{Si}_6\text{C}$ ( <b>c0</b> , $C_{5v}$ , $^1A_1$ )	2.62 (0.0)	5.64
	3.37 (30.6)	
	3.48 (0.0)	
$\text{Si}_6\text{N}$ ( <b>d0</b> , $C_{2v}$ , $^2A_2$ )	1.15 (0.0)	5.59 $\uparrow$ 4.33 $\downarrow$
	1.17 (0.7)	
	1.79 (9.7)	
$\text{Si}_6\text{O}$ ( <b>e0</b> , $C_1$ , $^1A$ )	2.40 (0.9)	5.43
	2.49 (3.6)	
	2.66 (11.8)	
$\text{Si}_7$ ( <b>f0</b> , $D_{5h}$ , $^1A_1'$ )	2.13 (0.0)	5.37
	2.19 (0.0)	
	2.31 (0.0)	

the HOMO–LUMO gaps drastically overestimate the energy of the lowest electronic transitions. High-symmetry structures exhibit several forbidden transitions. For instance, the first optically active state for  $\text{Si}_7$  is the seventeenth excited state at 3.35 eV with an oscillator strength  $f = 0.0082$ .

At the first glance, the spatial distributions of the HOMO and LUMO are very different for each cluster. Furthermore, the HOMOs are localized at the Si atoms and not on the dopant. Clusters with similar topological geometries show similar HOMOs, *i.e.*,  $\text{Si}_6\text{Be}$ ,  $\text{Si}_6\text{B}$ ,  $\text{Si}_6\text{C}$ , and  $\text{Si}_7$ . For  $\text{Si}_6\text{Be}$ ,  $\text{Si}_6\text{C}$ , and  $\text{Si}_7$ , the LUMOs are very similar, although the localization of the dopant atom within the cluster is different.

## D. Vibrational spectra

Fig. 3 shows the calculated vibrational spectra of the most stable isomers of  $\text{Si}_6\text{X}$  ( $X = \text{Si}, \text{C}, \text{O}, \text{Be}, \text{B}, \text{N}$ ), which are detailed in Table 2. Experimental spectra are available for  $\text{Si}_7$ ,  $\text{Si}_6\text{C}$ , and  $\text{Si}_6\text{O}$ , allowing for a comparison with the spectra of the predicted isomers (Fig. 3a–c). In all three cases, the spectrum of the lowest-energy isomer shows the best agreement to the experimental one (see Fig. S1–S5 in ESI† for further IR spectra of higher-energy isomers). The result for  $\text{Si}_7$  published earlier<sup>14</sup> is recalled here for completeness. The  $\text{Si}_7$  spectrum shows a single band at  $417 \text{ cm}^{-1}$  that has been assigned to the intense doubly degenerate  $e_1'$  mode of the highly symmetric  $D_{5h}$  pentagonal bipyramidal structure.

Replacing one Si by a C atom in pure  $\text{Si}_7$  significantly changes the IR–UV2CI spectrum (Fig. 3b). While the C-rich clusters prefer chain-like geometries, *e.g.*,  $\text{SiC}_6$ ,<sup>61</sup> stable Si-rich clusters have 3D structures. The predicted **c0** structure of  $\text{Si}_6\text{C}$  has  $C_{5v}$  symmetry, which is deformed from the  $D_{5h}$  structure of  $\text{Si}_7$  due to the greater strength of the C–Si bond *cf.* to Si–Si. The  $e_1'$  mode that dominates the spectrum of  $\text{Si}_7$  has its counterpart in the  $e_1$  mode for  $\text{Si}_6\text{C}$ . However, in  $\text{Si}_6\text{C}$  this mode is shifted to higher frequency, as it involves the lighter, but stronger bound C atom, and coincides with an intense  $a_1$  mode that is not IR active in  $\text{Si}_7$  (*cf.* Table 2). Together they can be assigned to the experimental band B. Similarly, the experimentally observed band A also corresponds to an  $a_1$  mode that is not IR active in the pure  $\text{Si}_7$  cluster. The band C at  $664 \text{ cm}^{-1}$  cannot be explained by the fundamental modes of the **c0** isomer, nor by any of the ten  $\text{Si}_6\text{C}$  isomers found within 1 eV in energy, suggesting that the band may be due to a combination band of the  $a_1$  mode at  $438 \text{ cm}^{-1}$  with the low frequency modes at  $231 \text{ cm}^{-1}$  ( $e_1$ ) or  $261 \text{ cm}^{-1}$  ( $a_1$ ). The 3D structure of the most stable  $\text{Si}_6\text{C}$  isomer is in good agreement with our earlier findings for  $\text{Si}_m\text{C}_n$  ( $m + n = 6$ ), where the first C atom does not change the topology of the geometry of the pure  $\text{Si}_6$  cluster.<sup>38</sup>

The spectrum of  $\text{Si}_6\text{O}$  is dominated by an intense absorption band (G) centered at about  $853 \text{ cm}^{-1}$ . Comparison with the calculated spectrum of the **e0** isomer shows that the band is due to the symmetric stretch mode of the Si–O–Si bridge

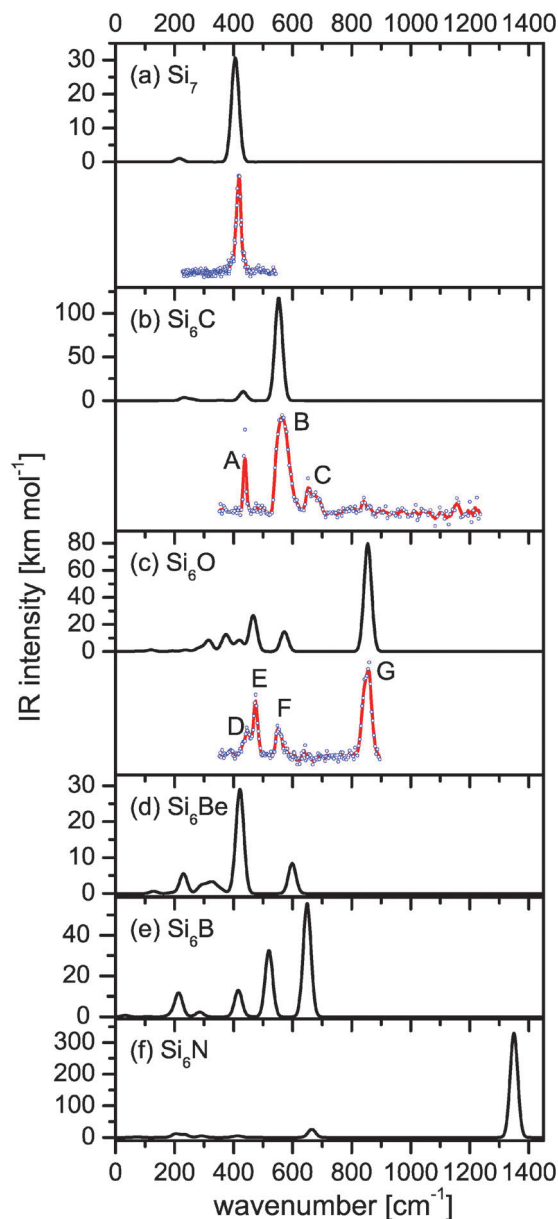


**Fig. 3** IR spectra of the most stable isomers of  $\text{Si}_6\text{X}$  clusters ( $\text{X} = \text{Si}, \text{C}, \text{O}, \text{Be}, \text{B}, \text{N}$ ) calculated at the B3LYP/cc-pVTZ level. The experimental IR spectra available for  $\text{Si}_7$  (from ref. 14),  $\text{Si}_6\text{C}$ , and  $\text{Si}_6\text{O}$  are obtained by the IR-UV2CI technique (blue dots: original data; red lines: three-point adjacent average). The measured IR intensities are given on a linear scale in arbitrary units. The experimental line positions (in  $\text{cm}^{-1}$ ) are 438 (A), 566 (B), 664 (C), 446 (D), 474 (E), 554 (F), and 853 (G).

predicted at  $855 \text{ cm}^{-1}$ . The asymmetric stretch vibration of the Si–O–Si unit is calculated at  $572 \text{ cm}^{-1}$  and can be assigned to the band F observed at  $554 \text{ cm}^{-1}$ .

For  $\text{Si}_6\text{Be}$ ,  $\text{Si}_6\text{B}$ , and  $\text{Si}_6\text{N}$ , no experimental IR spectra have been obtained so far, but the calculated spectra are included for completeness. We refrain from a more detailed discussion here, but only point to the intense high-frequency band predicted for  $\text{Si}_6\text{N}$  ( $1350 \text{ cm}^{-1}$ ). This vibration is characteristic of the isolated silaisonitrile ( $-\text{N}=\text{Si}$ ) group and can be compared to the Si–N stretch in  $\text{H}-\text{N}=\text{Si}$  found at  $\sim 1200 \text{ cm}^{-1}$ .<sup>62</sup>

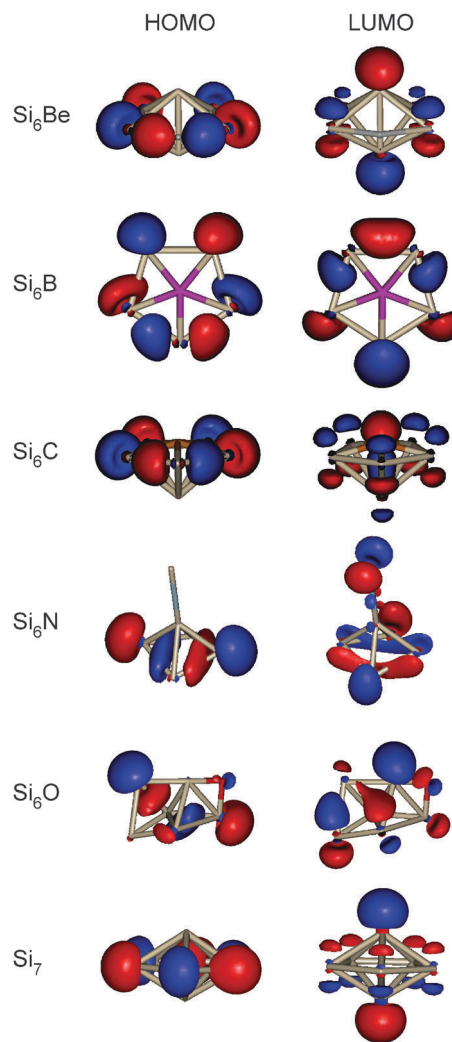


**Fig. 4** HOMO and LUMO orbitals of the ground state structures of  $\text{Si}_6\text{X}$  shown in Fig. 2 (a0–f0). The structural orientations are adjusted for a clear illustration of the orbitals.

## IV. Conclusions

In this study, neutral silicon clusters doped with the first row elements (B, C, N, O) have been generated in a laser vaporization source and characterized using time-of-flight mass spectrometry. The vibrational spectra of the C- and O-doped clusters have been measured using IR-UV2CI spectroscopy. The low energy structures of the  $\text{Si}_6\text{X}$  clusters doped with the first row elements Be–O have been investigated using DFT calculations. Candidate structures have been found using a DFT-based basin hopping global optimization scheme. In general, the most stable  $\text{Si}_6\text{X}$  structures and their IR spectra strongly depend on the dopant atom due to the effects arising from different size, mass, valency, and force fields. The calculations show that clusters doped with Be, B, or C favor structures based on the  $\text{Si}_7$  pentagonal bipyramid, with substitution of a single Si atom in either the ring (Be) or at an apex (B, C).  $\text{Si}_6\text{N}$  and  $\text{Si}_6\text{O}$ , however, exhibit completely different structures. By comparison between the measured IR spectra and the predicted ones,

the structures of  $\text{Si}_6\text{C}$  and  $\text{Si}_6\text{O}$  have been determined. We find good agreement between the experimental and the calculated spectra of the lowest-energy isomers. The calculated ionization energies also appear to be reliable, providing useful information for future experiments on, e.g., B and N doped clusters. Charge analysis with the natural bond orbital method shows that in all cases Si atoms act as electron donors within the clusters. As a general trend, doping of the  $\text{Si}_7$  cluster with first-row dopants is predicted to shift the optically allowed electronic transitions into the visible range, which is partly ascribed to symmetry reduction or the radical character of the doped cluster. In particular, the open-shell  $\text{Si}_6\text{B}$  and  $\text{Si}_6\text{N}$  clusters have predicted absorptions in the near-IR spectral range. These theoretical predictions will guide our efforts in recording optical spectra of these doped silicon clusters. In addition, experiments with the dual-target laser ablation source are envisaged to record vibrational spectra of  $\text{Si}_n\text{B}$ .

## Acknowledgements

This work was supported by the Deutsche Forschungsgemeinschaft within the research unit FOR 1282 (DO 729/5, FI 893/4). We gratefully acknowledge the support of the Stichting voor Fundamenteel Onderzoek der Materie (FOM) in providing beam time of FELIX and the FELIX staff for their skillful assistance, in particular, B. Redlich and A. F. G. van der Meer. The research leading to these results has received funding from the European Community's Seventh Framework Programme (FP7/2007–2013) under Grant Agreement No. 226716. We would like to acknowledge the collaboration with E. Janssens and P. Lievens using the dual target laser ablation cluster source. We thank C. Kerpel for fruitful discussion of the basin hopping technique.

## References

- V. Kumar, *Nanosilicon*, Elsevier Ltd, Oxford, 2007.
- H. F. Li, X. Y. Kuang and H. Q. Wang, Probing the structural and electronic properties of lanthanide-metal-doped silicon clusters:  $\text{M@Si}_6$  ( $\text{M} = \text{Pr}, \text{Gd}, \text{Ho}$ ), *Phys. Lett. A*, 2011, **375**, 2836–2844.
- S. Zhan, B. Li and J. Yang, Study of aluminum-doped silicon clusters, *Phys. B*, 2007, **387**, 421–429.
- A. Titov, F. Michelini, L. Raymond, E. Kulatov and Y. A. Uspenskii, Gap narrowing in charged and doped silicon nanoclusters, *Phys. Rev. B: Condens. Matter Mater. Phys.*, 2010, **82**, 235419.
- P. Karamanis, R. Marchal, P. Carbonniere and C. Pouchan, Doping-enhanced hyperpolarizabilities of silicon clusters: A global ab initio and density functional theory study of  $\text{Si}_{10}(\text{Li}, \text{Na}, \text{K})_n$  ( $n = 1, 2$ ) clusters, *J. Chem. Phys.*, 2011, **135**, 044511.
- L. Ma, J. Wang and G. Wang, Site-specific analysis of dipole polarizabilities of heterogeneous systems: Iron-doped  $\text{Si}_n$  ( $n = 1\text{--}14$ ) clusters, *J. Chem. Phys.*, 2013, **138**, 094304.
- V. T. Ngan, E. Janssens, P. Claes, J. T. Lyon, A. Fielicke, M. T. Nguyen and P. Lievens, High Magnetic Moments in Manganese-Doped Silicon Clusters, *Chem. – Eur. J.*, 2012, **18**, 15788–15793.
- J. De Haeck, S. Bhattacharyya, H. T. Le, D. Debruyne, N. M. Tam, V. T. Ngan, E. Janssens, M. T. Nguyen and P. Lievens, Ionization energies and structures of lithium doped silicon clusters, *Phys. Chem. Chem. Phys.*, 2012, **14**, 8542–8550.
- M. Jarrold, Nanosurface Chemistry on Size-Selected Silicon Clusters, *Science*, 1991, **252**, 1085–1092.
- M. B. Knickelbein, The infrared photodissociation spectra of  $\text{Fe}_n(\text{CH}_3\text{OH})_m$  complexes and their deuterated analogs near  $10\mu$ , *J. Chem. Phys.*, 1996, **104**, 3517–3525.
- P. Gruene, D. M. Rayner, B. Redlich, A. F. G. van der Meer, J. T. Lyon, G. Meijer and A. Fielicke, Structures of neutral  $\text{Au}_7$ ,  $\text{Au}_{19}$ , and  $\text{Au}_{20}$  clusters in the gas phase, *Science*, 2008, **321**, 674–676.
- M. Haertelt, J. T. Lyon, P. Claes, J. de Haeck, P. Lievens and A. Fielicke, Gas-phase structures of neutral silicon clusters, *J. Chem. Phys.*, 2012, **136**, 064301.
- G. von Helden, D. van Heijnsbergen and G. Meijer, Resonant ionization using IR light: A new tool to study the spectroscopy and dynamics of gas-phase molecules and clusters, *J. Phys. Chem. A*, 2003, **107**, 1671–1688.
- A. Fielicke, J. T. Lyon, M. Haertelt, G. Meijer, P. Claes, J. de Haeck and P. Lievens, Vibrational spectroscopy of neutral silicon clusters via far-IR-VUV two color ionization, *J. Chem. Phys.*, 2009, **131**, 171105.
- V. J. F. Lapoutre, M. Haertelt, G. Meijer, A. Fielicke and J. M. Bakker, Communication: IR spectroscopy of neutral transition metal clusters through thermionic emission, *J. Chem. Phys.*, 2013, **139**, 121101.
- A. Bekkerman, E. Kolodney, G. von Helden, B. Sartakov, D. van Heijnsbergen and G. Meijer, Infrared multiphoton ionization of superhot  $\text{C}_{60}$ : Experiment and model calculations, *J. Chem. Phys.*, 2006, **124**, 184312.
- F. Calvo and P. Parneix, Amplification of anharmonicities in multiphoton vibrational action spectra, *ChemPhysChem*, 2012, **13**, 212–220.
- G. Forte, G. G. N. Angilella, V. Pittala, N. H. March and R. Pucci, Neutral and cationic free-space oxygen-silicon clusters  $\text{SiO}_n$  ( $1 < n \leq 6$ ), and possible relevance to crystals of  $\text{SiO}_2$  under pressure, *Phys. Lett. A*, 2012, **376**, 476–479.
- H. Ning, H. Fan and J. Yang, Probing the electronic structures and properties of neutral and charged  $\text{CaSi}_n^-$  ( $n = 2\text{--}10$ ) clusters using Gaussian-3 theory, *Comput. Theor. Chem.*, 2011, **976**, 141–147.
- M. Jdraque and M. Martin, Charge-Transfer Processes in the Assembly of  $\text{Si}_n\text{O}_m$  Neutral Clusters, *J. Comput. Chem.*, 2011, **32**, 3497–3504.
- Y. S. Wang and S. D. Chao, Structures and Energetics of Neutral and Ionic Silicon-Germanium Clusters: Density Functional Theory and Coupled Cluster Studies, *J. Phys. Chem. A*, 2011, **115**, 1472–1485.
- H. Fan, Z. Ren, J. Yang, D. Hao and Q. Zhang, Study on structures and electronic properties of neutral and charged  $\text{MgSi}_n^-$  ( $n = 2\text{--}10$ ) clusters with a Gaussian-3 theory, *THEOCHEM*, 2010, **958**, 26–32.

- 23 Y. H. Zhu, B. X. Li, F. S. Liang and J. Xu, Theoretical Study of Neutral and Ionic  $\text{Si}_n\text{O}$  ( $n = 1-13$ ) Clusters, *Int. J. Mod. Phys. B*, 2009, **23**, 3527–3536.
- 24 M. C. Caputo, O. Ona and M. B. Ferraro, Theoretical prediction of atomic and electronic structure of neutral  $\text{Si}_6\text{O}_m$  ( $m = 1-11$ ) clusters, *J. Chem. Phys.*, 2009, **130**, 134115.
- 25 Y. Z. Lan and Y. L. Feng, Comparative study on the geometric and energetic properties, absorption spectra, and polarizabilities of charged and neutral  $\text{Cu}@Si_n$  clusters ( $n = 9-14$ ), *Phys. Rev. A: At., Mol., Opt. Phys.*, 2009, **79**, 033201.
- 26 D. Hossain, F. Hagelberg, C. U. Pittman, Jr. and S. Saebo, Structures and stabilities of clusters of  $\text{Si}_{12}$ ,  $\text{Si}_{18}$ , and  $\text{Si}_{20}$  containing endohedral charged and neutral atomic species, *J. Phys. Chem. C*, 2007, **111**, 13864–13871.
- 27 R. Zhao, Z. Ren, P. Guo, J. Bai, C. Zhang and J. Han, Geometries and electronic properties of the neutral and charged rare earth Yb-doped  $\text{Si}_n$  ( $n = 1-6$ ) clusters: A relativistic density functional investigation, *J. Phys. Chem. A*, 2006, **110**, 4071–4079.
- 28 C. Sporea, F. Rabilloud, A. R. Allouche and M. Frecon, Ab initio study of neutral and charged  $\text{Si}_n\text{Na}_p^+$  ( $n \leq 6$ ,  $p \leq 2$ ) clusters, *J. Phys. Chem. A*, 2006, **110**, 1046–1051.
- 29 B. X. Li, Stability of medium-sized neutral and charged silicon clusters, *Phys. Rev. B: Condens. Matter Mater. Phys.*, 2005, **71**, 235311.
- 30 A. Sieck, T. Frauenheim and K. Jackson, Shape transition of medium-sized neutral silicon clusters, *Phys. Status Solidi B*, 2003, **240**, 537–548.
- 31 C. Xiao, F. Hagelberg and W. Lester, Geometric, energetic, and bonding properties of neutral and charged copper-doped silicon clusters, *Phys. Rev. B: Condens. Matter Mater. Phys.*, 2002, **66**, 075425.
- 32 S. Nayak, B. Rao, S. Khanna and P. Jena, Atomic and electronic structure of neutral and charged  $\text{Si}_n\text{O}_m$  clusters, *J. Chem. Phys.*, 1998, **109**, 1245–1250.
- 33 M. Gomei, R. Kishi, A. Nakajima, S. Iwata and K. Kaya, Ab initio MO studies of neutral and anionic  $\text{SiC}_n$  clusters ( $n = 2-5$ ), *J. Chem. Phys.*, 1997, **107**, 10051–10061.
- 34 S. Wei, R. Barnett and U. Landman, Energetics and structures of neutral and charged  $\text{Si}_n$  ( $n \leq 10$ ) and sodium-doped  $\text{Si}_n\text{Na}$  clusters, *Phys. Rev. B: Condens. Matter Mater. Phys.*, 1997, **55**, 7935–7944.
- 35 K. Koyasu, M. Akutsu, M. Mitsui and A. Nakajima, Selective formation of  $\text{MSi}_{16}$  ( $M = \text{Sc}$ ,  $\text{Ti}$ , and  $\text{V}$ ), *J. Am. Chem. Soc.*, 2005, **127**, 4998–4999.
- 36 K. Koyasu, J. Atobe, M. Akutsu, M. Mitsui and A. Nakajima, Electronic and geometric stabilities of clusters with transition metal encapsulated by silicon, *J. Phys. Chem. A*, 2007, **111**, 42–49.
- 37 P. Claes, V. T. Ngan, M. Haertelt, J. T. Lyon, A. Fielicke, M. T. Nguyen, P. Lievens and E. Janssens, The structures of neutral transition metal doped silicon clusters,  $\text{Si}_n\text{X}$  ( $n = 6-9$ ;  $X = \text{V}$ ,  $\text{Mn}$ ), *J. Chem. Phys.*, 2013, **138**, 194301.
- 38 M. Savoca, A. Lagutschenkov, J. Langer, D. J. Harding, A. Fielicke and O. Dopfer, Vibrational Spectra and Structures of Neutral  $\text{Si}_m\text{C}_n$  Clusters ( $m + n = 6$ ): Sequential Doping of Silicon Clusters with Carbon Atoms, *J. Phys. Chem. A*, 2013, **117**, 1158–1163.
- 39 D. J. Harding, C. Kerpel, G. Meijer and A. Fielicke, Unusual Bonding in Platinum Carbido Clusters, *J. Phys. Chem. Lett.*, 2013, **4**, 892–896.
- 40 R. Gehrke and K. Reuter, Assessing the efficiency of first-principles basin-hopping sampling, *Phys. Rev. B: Condens. Matter Mater. Phys.*, 2009, **79**, 085412.
- 41 M. Haertelt, A. Fielicke, G. Meijer, K. Kwapien, M. Sierka and J. Sauer, Structure determination of neutral  $\text{MgO}$  clusters-hexagonal nanotubes and cages, *Phys. Chem. Chem. Phys.*, 2012, **14**, 2849–2856.
- 42 W. Bouwen, P. Thoen, F. Vanhoutte, S. Bouckaert, F. Despa, H. Weidele, R. Silverans and P. Lievens, Production of bimetallic clusters by a dual-target dual-laser vaporization source, *Rev. Sci. Instrum.*, 2000, **71**, 54–58.
- 43 D. Wales and J. Doye, Global optimization by basin-hopping and the lowest energy structures of Lennard-Jones clusters containing up to 110 atoms, *J. Phys. Chem. A*, 1997, **101**, 5111–5116.
- 44 M. Iwamatsu and Y. Okabe, Basin hopping with occasional jumping, *Chem. Phys. Lett.*, 2004, **399**, 396–400.
- 45 L. Zhan, J. Z. Y. Chen and W. K. Liu, Monte Carlo basin paving: An improved global optimization method, *Phys. Rev. E: Stat., Nonlinear, Soft Matter Phys.*, 2006, **73**, 015701.
- 46 M. T. Oakley, R. L. Johnston and D. J. Wales, Symmetrisation schemes for global optimisation of atomic clusters, *Phys. Chem. Chem. Phys.*, 2013, **15**, 3965–3976.
- 47 A. D. Becke, Density-functional exchange-energy approximation with correct asymptotic behavior, *Phys. Rev. A: At., Mol., Opt. Phys.*, 1988, **38**, 3098–3100.
- 48 J. P. Perdew, Density-functional approximation for the correlation energy of the inhomogeneous electron gas, *Phys. Rev. B: Condens. Matter Mater. Phys.*, 1986, **33**, 8822–8824.
- 49 F. Weigend, M. Haser, H. Patzelt and R. Ahlrichs, RI-MP2: optimized auxiliary basis sets and demonstration of efficiency, *Chem. Phys. Lett.*, 1998, **294**, 143–152.
- 50 M. J. Frisch, G. W. Trucks, H. B. Schlegel, G. E. Scuseria, M. A. Robb, J. R. Cheeseman, G. Scalmani, V. Barone, B. Mennucci, G. A. Petersson, H. Nakatsuji, M. Caricato, X. Li, H. P. Hratchian, A. F. Izmaylov, J. Bloino, G. Zheng, J. L. Sonnenberg, M. Hada, M. Ehara, K. Toyota, R. Fukuda, J. Hasegawa, M. Ishida, T. Nakajima, Y. Honda, O. Kitao, H. Nakai, T. Vreven, J. A. Montgomery, Jr., J. E. Peralta, F. Ogliaro, M. Bearpark, J. J. Heyd, E. Brothers, K. N. Kudin, V. N. Staroverov, R. Kobayashi, J. Normand, K. Raghavachari, A. Rendell, J. C. Burant, S. S. Iyengar, J. Tomasi, M. Cossi, N. Rega, J. M. Millam, M. Klene, J. E. Knox, J. B. Cross, V. Bakken, C. Adamo, J. Jaramillo, R. Gomperts, R. E. Stratmann, O. Yazyev, A. J. Austin, R. Cammi, C. Pomelli, J. W. Ochterski, R. L. Martin, K. Morokuma, V. G. Zakrzewski, G. A. Voth, P. Salvador, J. J. Dannenberg, S. Dapprich, A. D. Daniels, Ö. Farkas, J. B. Foresman, J. V. Ortiz, J. Cioslowski and D. J. Fox, *Gaussian 09 revision a.1*, Gaussian Inc., Wallingford, CT, 2009.
- 51 N. M. Tam, T. B. Tai and M. T. Nguyen, Thermochemical Parameters and Growth Mechanism of the Boron-Doped

- Silicon Clusters,  $\text{Si}_n\text{B}^q$  with  $n = 1-10$  and  $q = -1, 0, +1$ , *J. Phys. Chem. C*, 2012, **116**, 20086–20098.
- 52 J. Zh. Ye and B. X. Li, First-principles study on mixed  $\text{Si}_m\text{N}_n$  ( $m + n = 2-9$ ) clusters, *Comput. Theor. Chem.*, 2012, **992**, 84–91.
- 53 D. E. Goldberg, *Genetic algorithms in search, optimization, and machine learning*, Addison-Wesley Professional, New York, 1989.
- 54 O. Kostko, S. R. Leone, M. A. Duncan and M. Ahmed, Determination of ionization energies of small silicon clusters with vacuum ultraviolet radiation, *J. Phys. Chem. A*, 2010, **114**, 3176–3181.
- 55 K. Fuke, K. Tsukamoto, F. Misaizu and M. Sanekata, Near threshold photoionization of silicon clusters in the 248–146 nm region: Ionization potentials for  $\text{Si}_n$ , *J. Chem. Phys.*, 1993, **99**, 7807–7812.
- 56 J. Han and F. Hagelberg, A density functional theory investigation of  $\text{CrSi}_n$  ( $n = 1-6$ ) clusters, *Chem. Phys.*, 2001, **263**, 255–262.
- 57 A. E. Reed, R. B. Weinstock and F. Weinhold, Natural population analysis, *J. Chem. Phys.*, 1985, **83**, 735–746.
- 58 C. Xiao and F. Hagelberg, Charge transfer mechanism in Cu-doped silicon clusters: a density functional study, *THEOCHEM*, 2000, **529**, 241–257.
- 59 J. Han and F. Hagelberg, A density functional investigation of  $\text{MoSi}_n$  ( $n = 1-6$ ) clusters, *THEOCHEM*, 2001, **549**, 165–180.
- 60 J. Han, C. Xiao and F. Hagelberg, Geometric and electronic structure of  $\text{WSi}_N$  ( $N = 1-6, 12$ ) clusters, *Struct. Chem.*, 2002, **13**, 173–191.
- 61 V. Gordon, E. Nathan, A. Apponi, M. McCarthy, P. Thaddeus and P. Botschwina, Structures of the linear silicon carbides  $\text{SiC}_4$  and  $\text{SiC}_6$ : Isotopic substitution and Ab Initio theory, *J. Chem. Phys.*, 2000, **113**, 5311–5320.
- 62 M. Chen, A. Zheng, H. Lu and M. Zhou, Reactions of atomic silicon and germanium with ammonia: A matrix-isolation FTIR and theoretical study, *J. Phys. Chem. A*, 2002, **106**, 3077–3083.